ISSN : 0974 - 7486 Volume 8 Issue 9

Trade Science Inc.

Materials Science

An Indian Journal

Full Paper

MSAIJ, 8(9), 2012 [360-369]

A comparative investigation on optical, opto-thermal and mechanical properties of transparent semiconductor metal oxides

K.Boubaker

Equipe de Physique des dispositifs à Semiconducteurs, Faculté des Sciences de Tunis, Campus Universitaire 2092 Tunis, (TUNISIA)

E-mail: mmbb11112000@yahoo.fr

Received: 8th March, 2012 ; Accepted: 8th April, 2012

ABSTRACT

The λ-dependent optical refractive and extinction coefficients *n* and *k* of oxides thin layers (Sb_2O_4, SnO_2, ZnO and WO_3) have been determined from experimental measurement of reflection R(λ) and T(λ) transmission ratios within the Ultraviolet-Visible-Near-Infrared (UV/VIS/NIR) domain (300-1800nm). This study allowed deducing $\varepsilon_1(\lambda)$ and $\varepsilon_2(\lambda)$ expressions. Exploitation of results concerning their variations enabled estimating the plasma pulse ω_p, the relaxation time τ, the dielectric constant ε_+ and susceptibility χ_e. Furthermore, opto-thermal and mechanical investigations have been carried out and discussed relatively to the already established optical and thermal characteristics. Comparison confirmed the recently conjectured advantages of Sb_2O_4 in terms of both mechanical and electrical resistance

KEYWORDS

Sb_2O_4;
SnO_2;
ZnO;
WO_3;
Optical constants;
Opto-thermal expansivity ψ_{AB};
BPES;
Micro-hardness.

INTRODUCTION

Transparent conducting oxide (TCO) have been recently investigated for their interesting optical, mechanical and electrical performance[1-4]. The lastly recorded[5-14] optical transparence (up to 80%) in the visible domain, parallel to an good electrical conductivity[15,16] led to numerous applications of these materials in the new generation of opto-elecric devices[17-19].

Among the transparent conducting oxide (TCO) materials, indium oxide In_2O_3 has been widely used as a high-conductive, physically stable and chemically inert semi-conductor[20,21]. Thanks to its high transparency in the visible domain[22-24], In_2O_3 has been preferentially used in optoelectronic devices such as solar cells and liquid crystal displays. Nevertheless, its abundance decreased drastically (510 tons as reported by U.S. Geological Survey 2008) with the last decades' exploitation.

In this context, other relatively abundant metal-oxides have been tested and proposed as alternatives to In_2O_3 (TABLE 1[25])

TABLE 1 : Elements abundance in earth

Elements	Indium (In)	Antimony (Sb)	Tin (Sn)	Zinc (Zn)	Tungsten (W)
Earth's Crust Abundance (ppm)	0.05	0.2	2,2	75	160,6

This paper considers the fabrication and the comparative characterization of some oxides: ZnO,

SnO_2 WO_3 et Sb_2O_4 with perspectives for new related doped TCO materials[26,27].

These oxides, which are meant to replace the presently used In_2O_3, have wide bangaps (E_g>3eV)[36-40], and have been satisfactorily used as anti-reflection[28], anti-glare, anti-static and conductive materials[29-36].

Commonly, these oxides could be synthesized using several methods[35-44] like reactive evaporation, pulsed laser deposition (PLD), electron beam evaporation (EBE), chemical vapor deposition (CVD), sol-gel coating, and chemical spray pyrolysis.

In this paper, a global approach to identify physical constants of antimony (Sb), tin (Sn), zinc (Zn) and tungsten (W) non-doped oxides, fabricated using a low-cost spray pyrolysis setup, is used. Correlations between optical, optothermal and mechanical parameters have been proposed as guides for industrial application.

EXPERIMENT

Oxides preparation

ZnO SnO_2 and WO_3 thin layers have been prepared by the technique of chemical reactive technique in liquid phase spray. The obtained layers' structural and morphological properties, as well as synthesising details, have been recently published[45-47]

However, due to toxicity of antimony in a wet medium, antimony oxide thin layers were prepared by thermal evaporation followed by 24-hours annealing under air (not 2 hours as mentioned before[48]). The films were deposited on 1 x 2 cm^2 glass substrates. Sb (99.98 % of purity) thin films were obtained by evaporation in a HV chamber using a relatively low pressure of the order of 10^{-4}-10^{-5} Pa. Consecutively, the as-obtained Sb_2O_4 films were annealed in air atmosphere under temperatures varying between 400 °C and 550 °C.

Characterization techniques

The optical transmission and reflection measures has been achieved by means of a spectrophotometer (Shimadzu UV 3100S) dotted with an integrating sphere (LISR 3200). The spectrophotometer consists of double-beam monochromator with enough energy to make several types of accurate measures in a wide wave-length range (220-1800 nm). The morphological investigation along with hardness measurements have been performed in the MA2I Laboratory (ENIT, Tunisia). The tests consisted of hitting the targeted face of each sample by a common diamond-pyramidal-indenter under a prefixed load. The obtained imprints dimensions were subjected to geometrical standardized analyzes yielding a scaled value: the Micro-Hardness Vickers (Hv).

RESULTS AND DISCUSSION

Optical properties

Optical refractive index n(λ) and extinction coefficients k(λ)

Figures 1-a and 1-b show the optical transmission T(λ) and reflection R(λ) spectra in the Ultraviolet Visible Near Infrared (UV/VIS/NIR) domain.

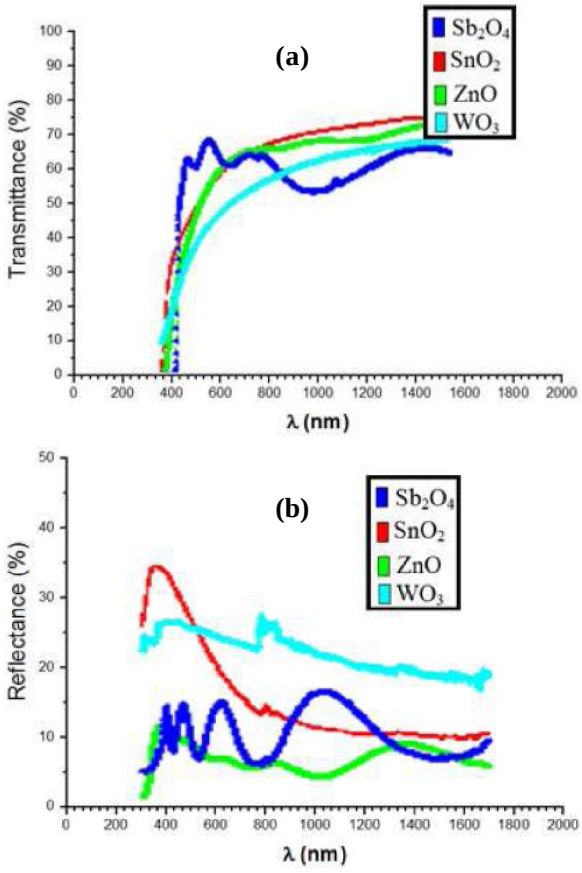

Figure 1 : R and T spectra of metal oxides thin films

Analysis of the obtained spectra and spectral lines data revealed that the four investigated materials are highly transparent in the Visible Near Infrared domain.

Full Paper

As expected, the oxides high optical transparency (H"80%) is a direct consequence of their wide bandgap.

The refractive index n(λ) and the extinction k(λ) were calculated using Mueller numerical method of resolution of nonlinear equation[49]. The calculated data of these coefficients are plotted in Figure 2-a,b,c,d.

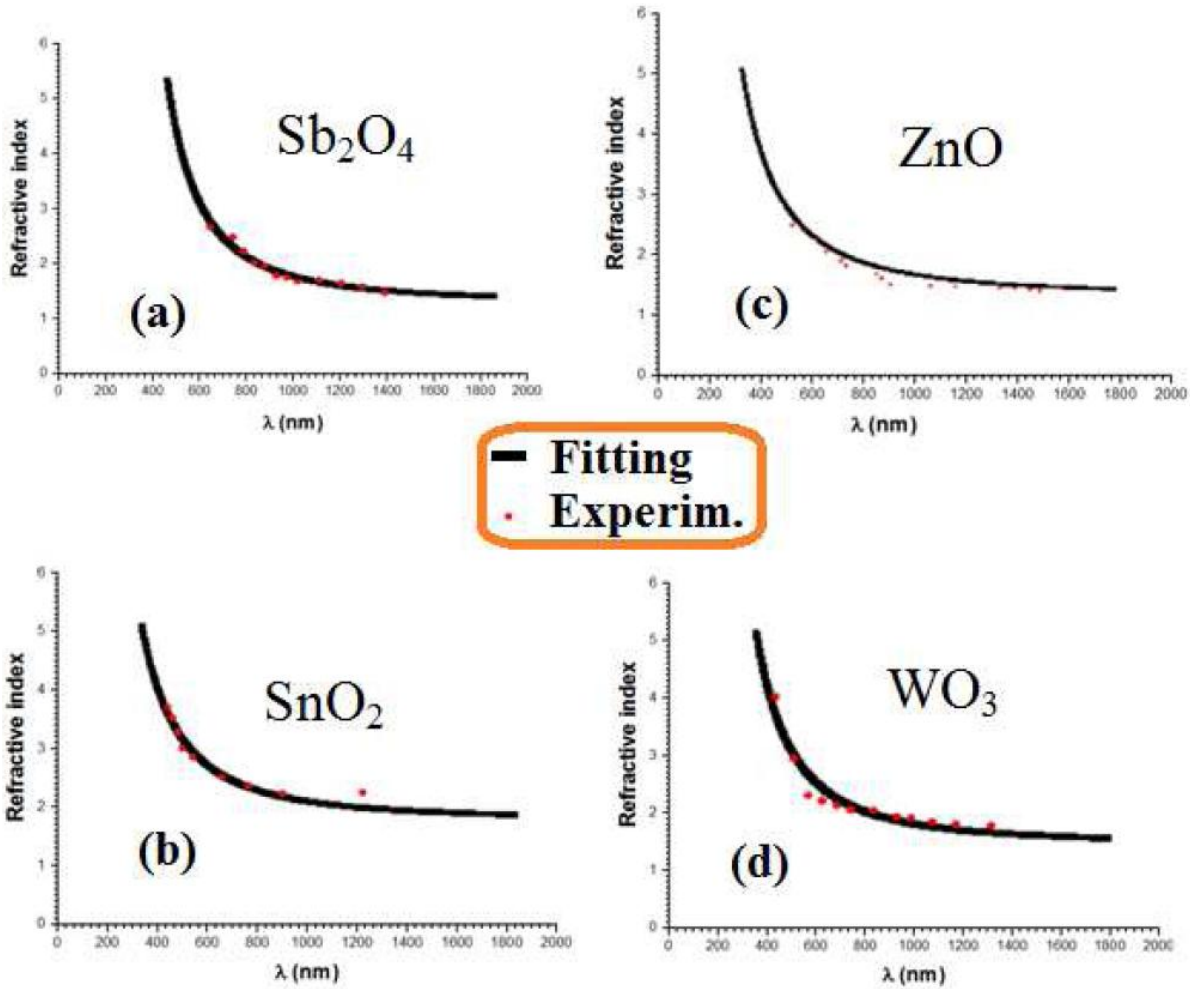

Figure 2 : Refractive index n

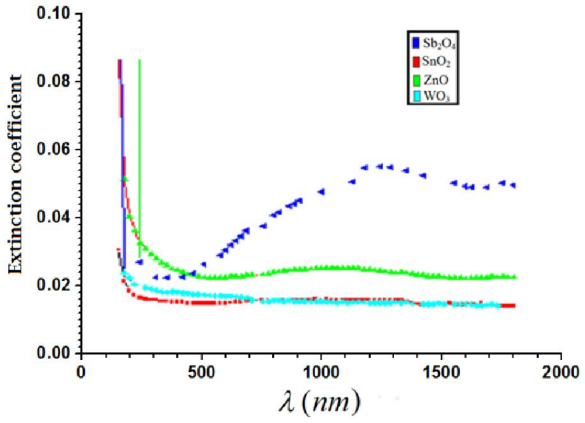

Figure 3 : Extinction coefficient *k*

The refractive index value varies in the range from 1.8 to 5.8 whereas the extinction coefficient varies in the domain [10^{-3}, 10^{-1}] for visible and near infrared regions. The λ-dependence behavior of the refractive index *n* is in good agreement with results reported previously on similar oxides[8,40,51]. The extinction coefficient *k* spectra, presented in Figure 3, show an obvious decrease versus wavelength except for ZnO layer. This exception is probably due to the excess of metal ions density.

In the same way, and for photons energies below the bandgap ($E < E_g$), the refractive index λ-dependency can be modelled using Cauchy[52] expression:

$$n(\lambda) = A + \frac{B}{\lambda^2} \quad (1)$$

Where A and B are constants.

Values of A and B, for each sample, along with other relevant constants, are presented in TABLE 2.

TABLE 2 : Values of A and B (Eq. 1) for each sample, along with other relevant constants

Oxyde	A	B(nm^2)	E_0(eV)	Ed(eV)	λ_0 (nm)	S_0(nm^{-2})	Eg(eV)
Sb_2O_4	1,616	339640,82	7.97	24.13	155.58	$1,25.10^{-4}$	3.92
SnO_2	1,565	127137,65	6.94	14.41	178.67	$65.04.10^{-4}$	3.60
ZnO	1,708	232395,57	6.56	14.38	189.02	$61.35.10^{-4}$	3.20
WO_3	1,749	271357,58	6.20	20.67	200.00	$83.34.10^{-4}$	3.30

Dielectric constants ε(λ), $\varepsilon_1(\lambda)$ $\varepsilon_2(\lambda)$ and $\chi_e(\lambda)$

Using the *n* and *k* calculated values, the dielectric constants $\varepsilon_1(\lambda)$ and $\varepsilon_2(\lambda)$ are deduced[53,54] according to the relations:

$$\begin{cases} \varepsilon(\lambda) = (n(\lambda) - ik(\lambda))^2 = \varepsilon_1(\lambda) + i\varepsilon_2(\lambda) \\ \begin{cases} \varepsilon_1(\lambda) = n(\lambda)^2 - k(\lambda)^2 \\ \varepsilon_2(\lambda) = 2n(\lambda)k(\lambda) \end{cases} \end{cases} \quad (2)$$

In the infrared region, where $\omega\tau << 1$ and $n^2 >> k^2$, $\varepsilon_1(\lambda)$ and $\varepsilon_2(\lambda)$ can be expressed in terms of the wavelength λ as[53]:

$$\begin{cases} \varepsilon_1(\lambda) = \varepsilon_\infty - \dfrac{\varepsilon_\infty \omega_p^2}{4\pi^2 c^2}\lambda^2 \\ \varepsilon_2(\lambda) = \dfrac{\varepsilon_\infty \omega_p^2}{4\pi^2 c^2 \tau}\lambda^3 \end{cases} \quad (3)$$

where τ is the relaxation time and ε_∞ is the high frequency limit-value of the dielectric constant.

In the same line, the plasma frequency ω_p is given by[54]:

$$\omega_p^2 = \frac{4\pi^2 N e^2}{\varepsilon_\infty m_e^*} \quad (4)$$

where : *N* is the charge carriers density and m_e^* is the la effective mass of the charge carrier.

The λ^2-dependent variation of $\varepsilon_1(\lambda)$ along with the λ^3-dependent variation of $\varepsilon_2(\lambda)$ are gathered in Figure 4-a,b and Figure 5-a,b

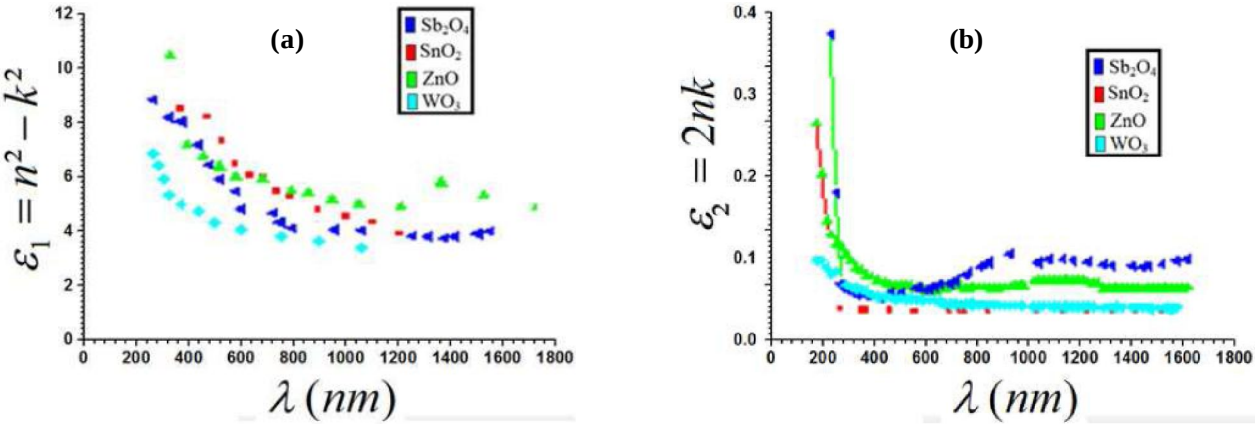

Figure 4 : Dielectric constant ε_1 and ε_2

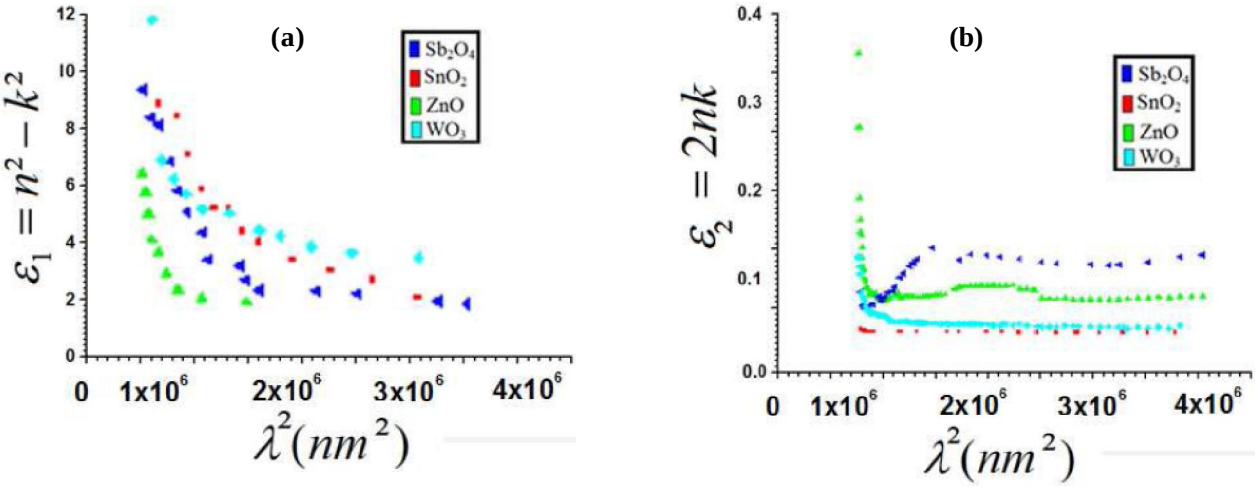

Figure 5 : Dielectric constant ε_1 and ε_2

Full Paper

The values of ε_∞ and ω_p deduced from Figure 5-a, along with those of τ deduced from Figure 5-b are presented in TABLE 3.

TABLE 3 : The values of the main parameters deduced from Figure 5-a and Figure 5-b

Oxyde	Eg(eV)	$\omega_p(10^{15}s^{-1})$	$\tau_{op}(10^{-14}s)$*	$\varepsilon(\infty)$	N/m^*10^{48} g^{-1} cm^{-3}	$-\chi_e$*
Sb_2O_4	3.92	1.024	3.55	6.0	2.177	0.4
SnO2	3.6	1.12	0.329	3.84	1.663	0.1
ZnO	3.2	1.158	0.103	4.719	2.185	0.13
WO3	3.3	0.941	0.353	5.915	1.0808	0.18

***The susceptibility values χ_e investigated at the extremes wavelength range**

***The relaxation time values τ_{op} investigated at the extremes wavelength range**

The λ-dependent expression of the dielectric susceptibility χ_e is deduced using the relation established by Spitzer *et al.*[55]:

$$\begin{cases}\chi_e = -\dfrac{Ne^2}{m_e^*\omega^2} \\ \varepsilon_\infty - \varepsilon_1 = -4\pi\chi_e\end{cases} \quad (5)$$

Figure 6 shows the variations of χ_e versus λ in the spectral range 600-1400 nm.

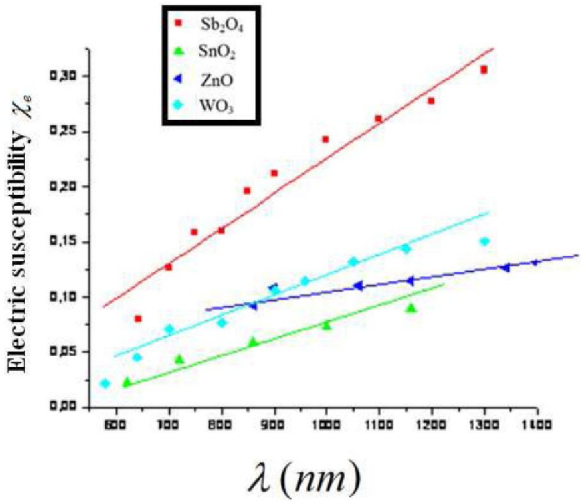

Figure 6 : Electric susceptibility χ_e

Finally, the studied samples refraction index dispersion has been studied using Wemple-DiDomenico model[56-64]. This dispersion is extremely relevant to communication and spectral analysis devices design. According to the model, the refractive index is linked to the photon energy through the expression:

$$\frac{1}{n^2-1} = \frac{E_0^2 - (h\nu)^2}{E_0 E_d} \quad (6)$$

where E_0 is the mono-oscillator energy and E_p is the dispersion energy (which measures transition intensity).

Figure 7 shows the linear variations of $(n^2 - 1)^{-1}$ versus $(h\nu)^2$ for the four samples. The values of E_0 and E_p were deduced, for each straight line, from the slope and the offset.

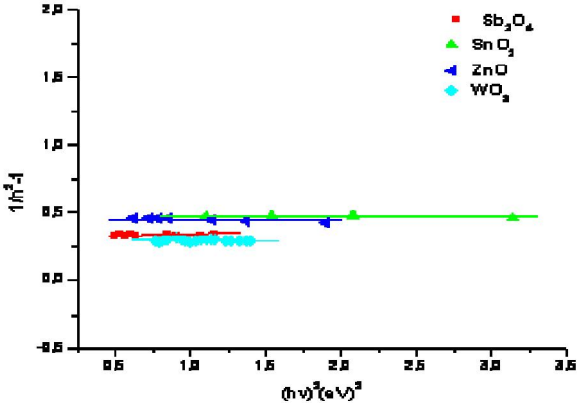

Figure 7 : Wemple-DiDomenico model

The mono-oscillator mean strength S_0 and the mean wavelength λ_0 have been defined through the relation:

$$\begin{cases}\dfrac{1}{n^2-1} = \left(1 - \dfrac{\lambda^2}{\lambda_0^2}\right)\left(S_0\lambda_0^2\right)^{-1} \\ E_0 = \dfrac{hc}{\lambda_0};\dfrac{E_d}{E_0} = S_0\lambda_0^2\end{cases} \quad (7)$$

Values of E_0, E_d, S_0 and λ_0, for each sample, are presented in TABLE 4. It has verified that the oscillator energy *E*o is an average empirical value which is the double of the optical band gap, E_{opt}, as obtained from the Wemple-Didomenico model[59-64].

TABLE 4 : Values of E_0, E_d, S_0 and λ_0, for the four oxides.

Oxyde	$\sigma_{dc}(\Omega cm)^{-1}$	$\sigma(0)_{op}$ (Ωcm^{-1})	$\tau_{op}(10^{-14}s)$
Sb_2O_4	19784.57	1876	3.55
SnO_2	1400.64	474	0.329
ZnO	576.14	941	0.103
WO_3	976.69	82.3	0.353

***The optical conductivity values σ_0 were investigated at the extreme wavelength range**

Optical conductivity $\sigma(\lambda)$

The optical conductivity $\sigma(\lambda)$ expression is deduced from the incident photons pulsation ω through the expression[65] of $\varepsilon(\omega)$:

$$\varepsilon(\omega) = \varepsilon_\infty - \frac{i\sigma(\lambda)}{\varepsilon_0\omega} \quad (8)$$

Using Eq. 2, it comes:

$$\sigma(\lambda) = \varepsilon_2\varepsilon_0 - \frac{2\pi c}{\lambda} \quad (9)$$

Figure 8 shows the variations of optical conductivity $\sigma(\lambda)$. It can be noticed that $\sigma(\lambda)$ and the wavelength vary in an opposite way. This feature can be attributed, for the four samples, to the high absorbance of the excited electrons.

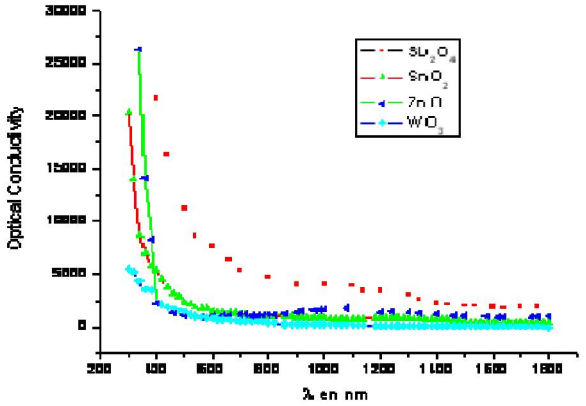

Figure 8 : Optical conductivity

The values of the optical conductivity σ_{dc} in the low-frequency region are compared to those given in the recent literature[66]:

$$\sigma_{dc} = \varepsilon_2\varepsilon_0 - \frac{Ne^2\tau}{m_e^*} \quad (10)$$

The critical values of the optical conductivity are presented in TABLE 5.

TABLE 5: Values of the Amlouk-Boubaker opto-thermal expansivity ψ_{AB}

Oxide	ZnO	SnO_2	WO_3	Sb_2O_4
ψ_{AB} ($10^{?12}$ $m^3 s^{?1}$)	18.22	23.80	7.32	10.00
Eg(eV)	3.2	3.6	3.3	3.92
Hv(Kg mm^{-2}) 1Hv=9.8MPa	232	368	754	775

Mechanical properties

The Micro-Hardness Vickers (Hv) set of measurements has been performed using a common diamond-pyramidal-indenter under a prefixed load (Figure 8). The obtained imprints dimensions have been exploited for yielding the Micro-Hardness Vickers (Hv) of each sample as a synthetic value. The obtained values are gathered in Figure 9.

The differences noticed in Figure 10 can be explained by the increase of the oxygen index, which is the highest in Sb_2O_4. This latter oxide relatively high hardness could also be attributed to presence of some lattice preferential orientations induced by annealing, as evoked in precedent sections. In fact, given that the Vickers tests are based on the resistance to direct penetration, the presence of c-axis oriented lattices (parallel to Vickers diamond-pyramidal-indenter direction, or perpendicular to the deposit plane) is favourable to increasing hardness.

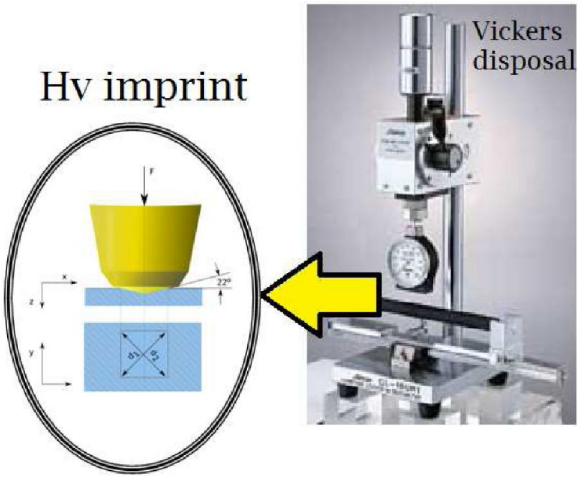

Figure 9 : Vickers hardness setup

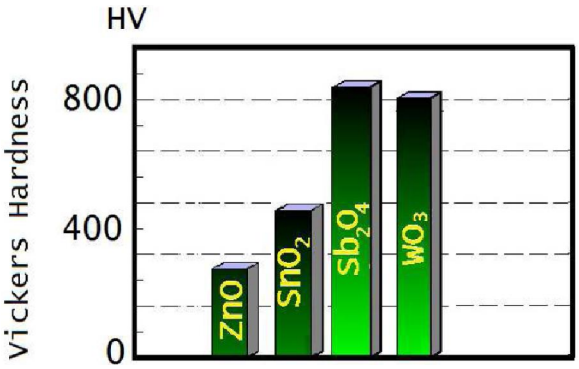

Figure 10 : Vickers hardness measurements

Opto-thermal study

Determination of the effective absorptivity $\hat{\alpha}$ using the BPES

The effective absorptivity $\hat{\alpha}$, has been defined in precedent studies[67,68] as the mean normalized absorbance weighted by $I(\tilde{\lambda})_{AM1.5}$, the solar standard irradiance:

$$\hat{\alpha} = \frac{\int_0^1 I(\tilde{\lambda})_{AM1.5} \times \alpha(\tilde{\lambda}) d\tilde{\lambda}}{\int_0^1 I(\tilde{\lambda})_{AM1.5} d\tilde{\lambda}} \quad (11)$$

where $I(\tilde{\lambda})_{AM1.5}$ is the Reference Solar Spectral

Full Paper

Irradiance, fitted using the Boubaker Polynomials Expansion Scheme BPES[69-83]:

$\mathbf{I(\tilde{\lambda}) = \left[\frac{1}{2N_0} \sum_{n=1}^{N_0} \theta_n . B_{4n}(\tilde{\lambda} \times \beta_n) \right]}$, where β_n are the Boubaker polynomials[73-83] B_{4n} minimal positive roots, θ_n are given coefficients, N_0 is a given integer, $\alpha(\tilde{\lambda})$ is the normalized absorbance spectrum and $\tilde{\lambda}$ **is the normalised wavelength:**

$$\begin{cases} \lambda \in [\lambda_{min}, \lambda_{max}] \Leftrightarrow \tilde{\lambda} \in [0,1] \\ \lambda_{min} = 300.0\,nm \ ; \lambda_{max} = 1800.0\,nm \end{cases} \quad (12)$$

The normalized absorbance spectrum $\alpha(\tilde{\lambda})$ is deduced from the BPES by establishing a set of *m* experimental measured values of the transmittance-reflectance vector $\left(T_i(\tilde{\lambda}_i); R_i(\tilde{\lambda}_i)\right)\Big|_{i=1..m}$ versus the normalized wavelength $\tilde{\lambda}_i\Big|_{i=1..m}$. Then the system (13) is set:

$$\begin{cases} R(\tilde{\lambda}) = \left[\frac{1}{2N_0} \sum_{n=1}^{N_0} \xi_n \times B_{4n}(\tilde{\lambda} \times \beta_n) \right] \\ T(\tilde{\lambda}) = \left[\frac{1}{2N_0} \sum_{n=1}^{N_0} \xi_n' \times B_{4n}(\tilde{\lambda} \times \beta_n) \right] \end{cases} \quad (13)$$

Where β_n are the 4n-Boubaker polynomials B_{4n} minimal positive roots[74,77], N_0 is a given integer and ξ_n and ξ_n' are coefficients determined through the Boubaker Polynomials Expansion Scheme BPES.

The normalized absorbance spectrum $\alpha(\tilde{\lambda})$ is deuced from the relation:

$$\alpha(\tilde{\lambda}) = \frac{1}{2d} \sqrt{\left(\ln \frac{1-R(\tilde{\lambda})}{T(\tilde{\lambda})} \right)^2 + \left(2 \ln \frac{1-R(\tilde{\lambda})}{\sqrt{T(\tilde{\lambda})}} \right)^2} \quad (14)$$

where *d* is the layer thickness.

The obtained value of normalized absorbance spectrum $\alpha(\tilde{\lambda})$ is a final guide to the determination of the effective absorptivity $\hat{\alpha}$ through (Eq. 11).

Determination of Amlouk-Boubaker opto-thermal expansivity ψ_{AB}

The Amlouk-Boubaker opto-thermal expansivity ψ_{AB} is a thermo-physical parameter defined in precedent studies[67-83], as a 3D expansion velocity of the transmitted heat inside the material. It is expressed in m^3s^{-1}, and calculated by:

$$\psi_{AB} = D/\hat{\alpha} \quad (15)$$

where *D* is the thermal diffusivity and $\hat{\alpha}$ is the effective absorptivity (§ *3.4.1.*).

The values of the calculated values of the Amlouk-Boubaker opto-thermal expansivity ψ_{AB}, for the four samples are gathered in TABLE 6.

TABLE 6 : Comparative hardness

Elements	Zn	Sn	W	Sb
Hardness Scale	Mohs: 2.5	Mohs: 1.5	Mohs: 7.5	Mohs: 3
	Brinell: 412 MNm^{-2}	Brinell: 51 MNm^{-2}	Brinell: 2570 MNm^{-2}	Brinell: 294 MNm^{-2}
			Vickers: 3430 MNm^{-2}	

DISCUSSION AND PERSPECTIVES

The optical transmittance of the elaborated oxides in the near infrared region, was of the order of 80 % and the band gap energy had an average value around 3.9 eV, which is conform to values yielded by similar techniques[84-88]. The refractive index, the dielectric constant as well as the plasma frequency of these oxides were also judged to be at close orders. Concerning the relaxation time, a high value has been recorded in the case of the antimony oxide Sb_2O_4.

Moreover, the mechanical and opto-thermal investigations results were in good agreement with both those deduced from the Wemple-Didomenico model[59-64] and some recently published results[45-49]. The relatively high c-axis oriented directions of grains of the samples with high oxygen indexes had indeed a benefit effect on their optothermal properties via low ψ_{AB} values.

Investigations led to spectacular conclusions concerning the antimony oxide Sb_2O_4: in fact, this oxide has the lowest value of the Amlouk-Boubaker opto-thermal expansivity ψ_{AB}, and the highest optical

conductivity parallel to a low thermal diffusivity. It is hence a promising transparent conducting material provided that an appropriate doping treatment is applied. The hardness performance of the oxides is also a determinant factor since these materials are more and more expected to ensure hardening glasses substrate and impeaching plastic layers inflammation

CONCLUSION

Oxides thin layers: Sb_2O_4, SnO_2, ZnO and WO_3 have been prepared using a low-cost protocol in air atmosphere. Appropriate comparative analyses and experimental measurement of reflection R(λ) and T(λ) transmission ratios within the Ultraviolet-Visible-Near-Infrared (UV/VIS/NIR) domain (300-1800nm) showed that Sb_2O_4 had the maximal optical conductivity due to its lowest extinction coefficient inside the visible domain. Moreover, it has been unexpectedly noticed that the microhardness of a given metal-oxide did not depend on the hardness of the metal itself. Hardness variation seemed to depend rather on the oxygen index (which is the highest for Sb_2O_4)

In summary, and besides positive features attributed to Sb_2O_4, the elaborated oxides have been comparatively judges as suitable to be used as powerful windows, and transparent conductor in many light-to-heat converters.

REFERENCES

[1] N.Kikuchi, E.Kusano, E.Kishio, A.Kinbara; Vacuum, **66**, 365-371 **(2002)**.

[2] R.B.Patil, R.K.Puri, Vijaya Puri; Journal of Alloys and Compounds, **462**, 235-239 **(2008)**.

[3] E.G-Berasategui, S.J.Bull, T.F.Page; Thin Solid Films, **447-448**, 26-32 **(2004)**.

[4] R.Thokala, J.Chaudhuri; Thin Solid Films, **266**, 189-191 **(1995)**.

[5] F.Yubero, V.M.Jime´nez, A.R.Gonzalez-Elipe; Surface Science, **400**, 116-126 **(1998)**.

[6] P.M.Gorley, V.V.Khomyak, S.V.Bilichuk, I.G.Orletsky, P.P.Horley, V.O.Grechko; Materials Science and Engineering, **B 118**, 160-163 **(2005)**.

[7] D.Davazoglou, A.Donnadieu; Thin Solid Films, **147**, 131-142 **(1987)**.

[8] S.W.Xue, X.T.Zu, W.L.Zhou, H.X.Deng, X.Xiang, L.Zhang, H.Deng; Journal of Alloys and Compounds, **448**, 21-26 **(2008)**.

[9] A.Mosbah, T.A.Moustaghfir, S.Abed, N.Bouhssira, M.S.Aida, E.Tomasella, M.Jacquet; Surface & Coatings Technology, **200**, 293-296 **(2005)**.

[10] D.F.Paraguay, L.W.Estrada, N.D.R.Acosta, E.Andrade, M.Miki-Yoshida; Thin Solid Films, **350**, 192-202 **(1999)**.

[11] J.C.Manifacier; Thin Solid Films, **90**, 297-308 **(1982)**.

[12] T.Serin, N.Serin, S.Karadeniz, H.Sarý, N.Tugluoglu, O.Pakma; Journal of Non-Crystalline Solids, **352**, 209-215 **(2006)**.

[13] Y.Villachon-Renard, G.Leveque, A.Abdellaoui, A.Donnadieu; Thin Solid Films, **203**, 33-39 **(1991)**.

[14] M.Regragui, V.Jousseaume, M.Addou, A.Outzourhit, J.C.Berne´de, B.El Idrissi; Thin Solid Films, **397**, 238-243 **(2001)**.

[15] T.Minami, T.Miyata; Thin Solid Films, **517**, 1474-1481 **(2008)**.

[16] E.Fortunato, R.Martins; Thin Solid Films, **511**, 295-302 **(2005)**.

[17] T.Minami, Y.Mochizuki, T.Miyata; Thin Solid Films, **494**, 33-39 **(2006)**.

[18] E.Elangovan, K.Ramamurthi; Journal of Optoelectronics and Advanced Materials, **5(1)**, 45-54, March **(2003)**.

[19] G.X.Liu, F.K.Shan, W.J.Lee, B.C.Shin, H.S.Kim, J.H.Kim; Ceramics International, **34**, 1011-1015 **(2008)**.

[20] V.Senthilkumar, P.Vickraman; Current Applied Physics, **10**, 880-885 **(2010)**.

[21] S.Parthiban, E.Elangovan, K.Ramamurthi, R.Martins, E.Fortunato; Solar, Energy Materials & Solar Cells, **94**, 406-412 **(2010)**.

[22] S.P.Singh, L.M.Tiwari, O.P.Agnihotri; Thin Solid Films, **139**, 1-7 **(1986)**.

[23] J.Joseph Prince, S.Ramamurthy, B.Subramanian, C.Sanjeeviraja, M.Jayachandran; Journal of Crystal Growth, **240**, 142-151 **(2002)**.

[24] Periodic Table of Elements, Site Web: Enviromentalchemistry.com

[25] Y.Furubayashi, T.Hitosugi, Y.Yamamoto, Y.Hirose, G.Kinoda, K.Inaba, T.Shimada, T.Hasegawa; Thin Solid Films, **496**, 157-159 **(2006)**.

[26] A.N.Banerjee, K.K.Chattopadhyay; Progress in Crystal Growth and Characterization of Materials, **50**, 52-105 **(2005)**.

[27] Gyeong-Su Park; Surface and Coatings Technology, **115**, 52-56 **(1999)**.

[28] A.Galdikas, A.Mironas, D.Senulienc, A.S˘etkus; Thin Solid Films, **323**, 275-284 **(1998)**.

[29] A.Labidi, E.Gillet, R.Delamare, M.Maaref, K.Aguir; Sensors and Actuators B, **120**, 338-345 **(2006)**.

[30] H.Hallil, P.Ménini, H.Aubert; Procedia Chemistry, **1**, 935-938 **(2009)**.

[31] J.Bandara, C.M.Divarathne, S.D.Nanayakkara; Solar Energy Materials & Solar Cells, **81**, 429-437 **(2004)**.

[32] A.Alkaya, R.Kaplan, H.Canbolat, S.S.Hegedus; Renewable Energy, **34**, 1595-1599 **(2009)**.

[33] Ki-Won Kim, Pyeong-Seok Cho, Sun-Jung Kim, Jong-Heun Lee, Chong-Yun Kang, Jin-Sang Kim, Seok-Jin Yoon; Sensors and Actuators B, **123**, 318-324 **(2007)**.

[34] G.Leo, R.Rella, P.Siciliano, S.Capone, J.C.Alonso, V.Pankov, A.Ortiz; Sensors and Actuators B, **58**, 370-374 **(1999)**.

[35] J.Montero, J.Herrero, C.Guillén; Solar Energy Materials & Solar Cells, **94**, 612-616 **(2010)**.

[36] T.Prasada Rao, M.C.Santhoshkumar; Applied Surface Science, **255**, 4579-4584 **(2009)**.

[37] T.Ratana, P.Amornpitoksuk, T.Ratana, S.Suwanboon; Journal of Alloys and Compounds, **470**, 408-412 **(2009)**.

[38] Abdul Faheem Khan, Mazhar Mehmood, Muhammad Aslam, Muhammad Ashraf; Applied Surface Science, **256**, 2252-2258 **(2010)**.

[39] Ebru S¸enadım, Sıtkı Eker, Hamide Kavak, Ramazan Esen; Solid State Communications, **139**, 479-484 **(2006)**.

[40] X.Q.Wei, J.Z.Huang, M.Y.Zhang, Y.Du, B.Y.Man; Materials Science and Engineering B, **166**, 141-146 **(2010)**.

[41] G.X.Liu, F.K.Shan, W.J.Lee, B.C.Shin, H.S.Kim, J.H.Kim; Ceramics International, **34**, 1011-1015 **(2008)**.

[42] J.Szuber, G.Czempik, R.Larciprete, B.Adamowicz; Sensors and Actuators B, **70**, 177-181 **(2000)**.

[43] Jae-Ho Chung, Yong-Sahm Choe, Dae-Seung Kim; Thin Solid Films, **349**, 126-129 **(1999)**.

[44] A.Amlouk, K.Boubaker, M.Amlouk; Journal of Alloys and Compounds, **490**, 602-604 **(2010)**.

[45] A.Amlouk, K.Boubaker, M.Amlouk, M.Bouhafs; Journal of Alloys and Compounds, **485**, 887-891 **(2009)**.

[46] S.Dabbous, T.Ben Nasrallah, J.Ouerfelli, K.Boubaker, M.Amlouk, S.Belgacem; Journal of Alloys and Compounds, **487**, 286-292 **(2009)**.

[47] B.Ouni, J.Ouerfelli, A.Amlouk, K.Boubaker, M.Amlouk; Journal of Non-Crystalline Solids, **356**, 1294-1299 **(2010)**.

[48] S.Belgacem, R.Bennaceur; Rev.Phys.Appl., **25**, 1245 **(1990)**.

[49] F.Yakuphanoglu, A.Cukurovali, I.Yilmaz; Optical Materials, **27**, 1363-1368 **(2005)**.

[50] A.Szekeres, D.Gogova, K.Gesheva; J.of Crystal Growth, **198/199**, 1235-1239 **(1999)**.

[51] H.G.Tompkins, W.A.McGahan; Spectroscopic Ellipsometry and Reflectometry, John Wiley & Sons Inc., New York, **(1999)**.

[52] M.Sesha Reddy, K.T.Ramakrishna Reddy, B.S.Naidu, P.J.Reddy; Optical Materials, **4**, 787-790 **(1995)**.

[53] J.I.Pankove; 'Optical Processes in Semiconductors', Prentice-Hall, New Jersey, 92 **(1971)**.

[54] W.G.Spitzer, H.Y.Fan; Physical Review, **106(5)**, 882 **(1957)**.

[55] S.H.Wemple, M.DiDomenico; Phy.Rev.B, **1**, 193-202 **(1970)**.

[56] S.H.Wemple, M.DiDomenico; Phy.Rev.B, **3**, 1338-1351 **(1971)**.

[57] S.H.Wemple, M.DiDomenico; Phy.Rev.Lett., **23**, 1156-1162 **(1971)**.

[58] S.H.Wemple, M.DiDomenico; J.Appl.Phys., **40**, 720-731 **(1969)**.

[59] S.H.Wemple, M.DiDomenico; Phys.Rev., **B7**, 3767-3777 **(1973)**.

[60] S.H.Wemple, M.DiDomenico; J.Chem.Phys., **67**, 2151-2166 **(1977)**.

[61] G.Galeczki; Infrared Physics, **31(3)**, 215-217 **(1991)**.

[62] S.H.Wemple; Solid State Comm., **12(7)**, 701-704 **(1973)**.

[63] M.DiDomenico Jr., M.Eibschütz, H.J.Guggenheim, I.Camlibel; Solid State Comm., **7(16)**, 1119-1122 **(1969)**.

[64] J.I.Pankove; Optical Processes in Semiconductors, Dover Publications, Inc., New York, **(1975)**.

[65] François Gervais; Materials Sciences and Engineering R, **39**, 29-92 **(2002)**.

[66] S.Lazzez, K.B.Ben Mahmoud, S.Abroug, F.Saadallah, M.Amlouk; Current App.Physics, **9**, 1129-1134 **(2009)**.

[67] K.B.Ben Mahmoud, M.Amlouk; Materials Lett., **63**, 991-999 **(2009)**.

[68] K.B.Ben Mahmoud; J.of Thermoph.and Heat Trans., **23**, 409-421 **(2009)**.

[69] T.G.Zhao, Z.S.Wang, K.B.Ben Mahmoud; Int.J.of Math.Comp., **1**, 13-20 **(2008)**.
[70] K.Boubaker; Trends in App.Sc.Research, **2**, 540-544 **(2007)**.
[71] K.Boubaker; Num.Methods for Partial Diff.Eq.NMPDE, **25**, 802-811 **(2009)**.
[72] S.Slama, J.Bessrour, B.Karem, M.Bouhafs; Proc.of COTUME'08, 79-88 **(2008)**.
[73] A.Belhadj, J.Bessrour, M.Bouhafs, L.Barrallier; J.of Therm.Anal.Calorim., **97**, 911-922 **(2009)**.
[74] O.B.Awojoyogbe, K.Boubaker; Curr.App.Phys., **9**, 278-288 **(2009)**.
[75] J.Ghanouchi, H.Labiadh, K.Boubaker; Int.J.of Heat and Techn., **26**, 49-57 **(2008)**.
[76] S.Slama, M.Bouhafs, K.B.Ben Mahmoud; Int.J.of Heat and Techn., **26**, 141-152 **(2008)**.
[77] K.Boubaker; Far-East.J.of App.Math., **31**, 299-302 **(2008)**.
[78] D.H.Zhang, F.W.Li; IJAPLett., **2**, 25-33 **(2009)**.
[79] S.Tabatabaei, T.Zhao, O.Awojoyogbe, F.Moses; Heat Mass Transf., **45**, 1247-1252 **(2009)**.
[80] S.Fridjine, M.Amlouk; Modern Phys.Lett.B, **23**, 2179-2188 **(2009)**.
[81] O.D.Oyodum, O.B.Awojoyogbe, M.Dada, J.Magnuson; Europ.Phys.J.-Appl.Phys., **46**, 21201-21211 **(2009)**.
[82] A.Belhadj, O.Onyango, N.Rozibaeva; J.Thermophys. Heat Transf., **23**, 639-653 **(2009)**.
[83] P.Nunes, B.Fernandes, E.Fortunato, P.Vilarinho, R.Martins; Thin Solid Films, **337**, 176-179 **(1999)**.
[84] P.Nunes, E.Fortunato, A.Lopes, R.Martins; Int.J.of Inorganic Materials, **3**, 1129-1131 **(2001)**.
[85] P.Nunes, A.Malik, B.Fernandes, E.Fortunato, P.Vilarinho, R.Martins; Vacuum, **52**, 45-49 **(1999)**.
[86] P.Nunes, E.Fortunato, R.Martins; Thin Solid Films, **383**, 277-280 **(2001)**.
[87] P.Nunes, E.Fortunato, R.Martins; Int.J.of Inorganic Materials, **3**, 1125-1128 **(2001)**.
[88] P.Nunes, E.Fortunato, P.Vilarinho, R.Martins; Int.J.of Inorganic Materials, **3**, 1211-1213 **(2001)**.